European Journal of Wood and Wood Products (2025) 83:139
https://doi.org/10.1007/s00107-025-02285-1

ORIGINAL ARTICLE

Influence of surface preparation and surface topography on tensile shear strength of polyurethane adhesively bonded beech wood single-lap joints: a finite element method approach

Luka Naumovski[1] · Martin Capuder[1] · Jakub Sandak[2] · Boris Azinović[1]

Received: 23 February 2025 / Accepted: 5 June 2025

Abstract

In this study, the mechanical properties of bonded single-lap joints are analysed by tensile lap shear tests on beech wood. A one-component polyurethane adhesive was used, and three different methods of surface preparation were applied: planing, sanding along the grain, and sanding perpendicular to the grain. Prior to bonding, the wooden lamellae underwent laser scanning to obtain surface profiles, which were then analysed for surface roughness. Scanned surface topographies with their features were integrated into the finite element analysis (FEA) software COMSOL Multiphysics to simulate the lap shear bonding area for different surface profiles and roughness. The FEA model implements linear material models, which represent the adherend and thin adhesive layer, combined with a modified local cohesive zone model for the adhesive bond interfacial forces. The experimental tests were conducted in a dry environment, where a higher surface roughness achieved by sanding correlated with a higher tensile shear strength. This increased surface roughness was attributed to the enhanced mechanical interlocking mechanism. This finding aligns with the FE analysis, which showed that increased surface roughness, micropillars and indentations, led to variations in stress concentration and distribution compared to a smooth surface bond.

1 Introduction

Bonding of wood is a crucial process in the wood processing industry, especially as interest in timber buildings is rising (Ammann 2015). In Slovenia, it is expected that by 2030, each public building will contain at least 30% wood or wood products. This goal is part of a broader strategy to increase the sustainability of construction practices and reduce the environmental impact of the building sector (Government of the Republic of Slovenia 2023). Currently, the majority of timber used for structural purposes in Slovenia comprises coniferous species, predominantly spruce/fir. However, due to environmental concerns and climate change, the forest composition is currently changing towards broadleaved species among which European beech (*Fagus* sp.) will play a significant role in the future. In this regard, beech has become the most represented wood species in Slovenian forests (Plos et al. 2022). Traditionally used as firewood, beech's superior mechanical properties indicate its potential for structural applications. According to German technical approval (Z-9.1-679 2018), both spruce/beech and beech glued laminated timber (GLT) are approved for use in structural applications within Service Class 1, in accordance with DIN EN 1995-1-1. Nonetheless, due to its higher density and dimension instability compared to widely used softwoods, beech faces challenges in passing tests for structural adhesives (Pramreiter and Grabner 2023).

Adhesive bond is the most frequent connection to form wood composite materials (WBCs) and it also plays a significant role in the performance of the whole material. Nevertheless, there is a big knowledge gap regarding the impact of complex loads on the bond performance between beech-wood and adhesive. Adhesive-wood complex is a very complicated mechanical system where many local events such as non-uniform cracking in adherend/adhesive occur when exceeding bearing capacity. For successful bonding, several factors need to be accounted for, with surface roughness

✉ Boris Azinović
boris.azinovic@zag.si

[1] Slovenian National Building and Civil Engineering Institute, Dimičeva ulica 12, Ljubljana 1000, Slovenia

[2] InnoRenew CoE, Livade 6a, Izola 6310, Slovenia

Published online: 19 July 2025

being just one of them (Hänsel et al. 2022). In this context, a comprehensive theoretical review of surface texture and its impact on the mechanical performance of bonded joints across various materials is presented by Naat et al. (2021). The review introduces and discusses phenomena such as mechanical interlocking and surface classification, as well as possible effects on wettability. Contrary, Budhe et al. (2015) experimentally investigated the influence of surface roughness on adhesive bond strength using different adherend materials, including wood and aluminium. Finally, mechanics of adhesive interactions and mechanical interlocking in wood are briefly discussed in Gardner et al. (2014), where the basic concepts of interlocking, as firstly proposed by McBain and Hopkins (1925), divided into two groups, specifically: locking by friction and locking by dovetailing, are introduced.

Surface roughness is commonly associated with mechanical interlocking, but it is still unclear how much strength it provides (Niemz et al. 2023). Furthermore, Hänsel et al. (2023) suggest when a limit value of roughness is exceeded, a positive effect cannot be realized. Consequently, several studies have been conducted on surface preparation of beech wood, with the most effective method found to be the application of a water solution of primer before bonding (Kläusler et al. 2014a; Konnerth et al. 2016; Luedtke et al. 2015). Since the activation time of primer and the double press time need to be accounted for, a study by Bamokina Moanda et al. (2022) suggested using micro-structured knives for planing, however no positive influence on bond strength was reported. The results of their study were also in agreement with Ammann et al. (2016), who suggested that wood failure percentage (WFP) cannot be influenced by machining method.

Generally, in an adhesive bond two main forces could be distinguished, i.e., cohesive and adhesive forces, the former being related only to the nature of the material, and the later defining the complex interaction between the adhesive and adherend, strongly affected by the contact surface morphology. Consequently, as the roughness of the surface increases, the number of indentations in which the adhesive can penetrate is greater. Following, surface with an optimal roughness, when compared to a completely smooth surface, can make the bond reach a higher strength. Nevertheless, the realization of an optimally rough surface geometry is not that straightforward, as small indentations can lead for the adhesive not to fill them completely and air bubbles to be trapped inside the cavity, which consequently results in a weakened bond. In this regard, three primary failure patterns are commonly observed: cohesive (material) fracture – crack propagates through the adhesive layer and causes the adhesive layer to remain on both surfaces of adhesion or crack propagates through the adherend (cohesive failure in wood material), adhesive (interfacial) fracture – failure of the interfacial bond between the adhesive and the adherend, and a mixed-pattern fracture – combined cohesive-adhesive failure. In this regard, predicting and observing the mechanical response of composites and structural elements with experiments usually does not provide full insight into the local mechanical behaviour or behaviour on a micro level, which could be of crucial influence for interpretation of the results.

For better understanding of mechanical behaviour and more accurate predictions, studies on smaller specimens in combination with finite element modelling are necessary. In recent years, studies on modelling adhesively bonded joints in mode I and mode II have been conducted by various authors (Clerc et al. 2019; De Moura et al. 2011; Fernandes et al. 2013; Gliszczynski 2021; Gómez-Royuela et al. 2022; Sebera et al. 2021). In the afore listed studies, no surface roughness or topography were included in the model. Following, to this end this is the first study to investigate surface preparation and mechanical interlocking of beech wood joints through experimental tests combined with finite element (FE) analysis. Therefore, the following study focuses on the investigation of beechwood-adhesive bondline using so-called morphological FE modeling, where the FE model includes the effects of surface topography and roughness (mechanical interlocking) on general stiffness and strength of the bondline. On the other hand, no penetration of the adhesive was implemented, as studied by Hammerquist and Nairn (2018).

2 Materials and methods

2.1 Specimens preparation

Defect-free boards of European beech (*Fagus sylvatica* L.) with grain angle orientation between 30° and 85° were selected for specimen preparation. To minimize density variation, all lamellae were sawn from the same board. After resawing, the lamellae were conditioned in a climate-controlled room at 20 °C and 65% relative humidity until they reached a moisture content of approximately 12%. The wood density, determined from offcuts after resawing, was 700 ± 20 kg/m³. The lamellae were then planed to final thicknesses of 5.0 and 5.5 mm. A portion of the 5.5 mm-thick lamellae was further sanded along (sanded 0°) and across (sanded 90°) the grain to a final thickness of ~5.0 mm. Sanding was performed using a VOLPATO LBK150 edge belt sander with P120 grit sandpaper. Finally, only representative, defect-free samples, were used for bonding and subsequent topography analysis. There were no local grain deviations or similar irregularities observed.

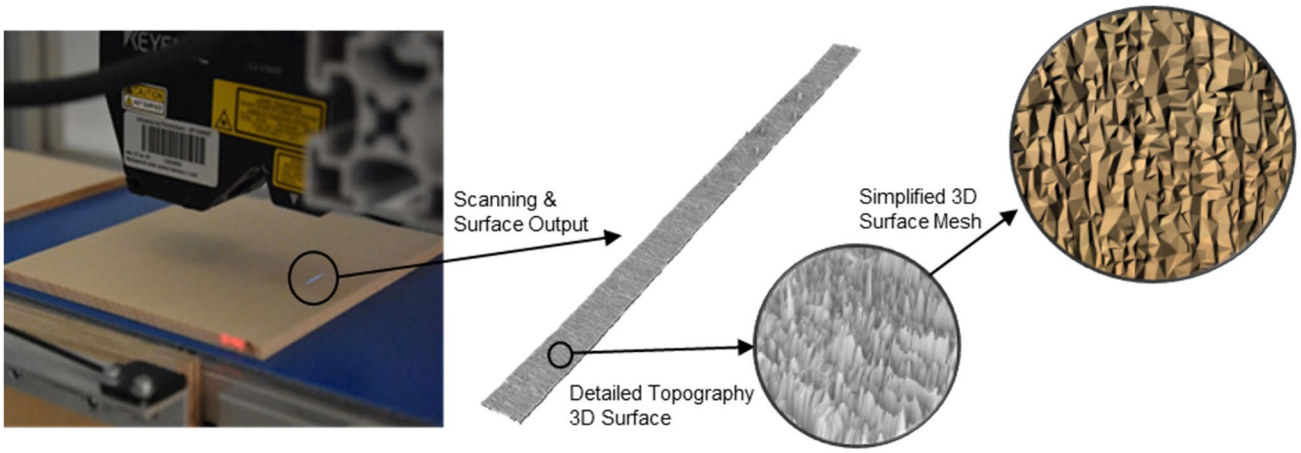

Fig. 1 Scanning procedure of lamellae surface profile. Blue line on the lamellae represents a scanned surface width of approximately 7 mm

Table 1 Adhesive properties and bonding conditions

Type of applied adhesive	1 C-PUR, Loctite HB S209
Amount of applied adhesive	180 g/m^2 (one side application)
Device pressure	1 MPa
Press time	90 min

2.2 Scanning procedure

The lamellae underwent scanning of their surface profile with Keyence LJ-7020 laser profiler where approximately 7 mm of surface along the lamellae was scanned, the area intended for bonding of specimens, as shown in Fig. 1. Both sides of the lamellae were scanned and immediately after the scanning process, the lamellae were bonded together. No primer or water spray before scanning and bonding was used since only different surface preparation methods and their influence were studied, both of which would influence bond strength (Kläusler et al. 2014a).

3D surface roughness was assessed on the custom-made scanner containing the numerically controlled conveyor belt and 2D blue laser displacement sensor. The stepper motor of the conveyor belt allowed precise control of the sample position under the sensor and provided a trigger for the surface profile acquisition. The Keyence LJ-V7020 sensor controlled by the XG-X2800LJ unit resulted in a spatial resolution of the surface topography of 6.8 µm. The declared vertical repeatability of the sensor was 0.2 µm. The feed speed of the conveyor belt during surface profile acquisition was 2 m/min while the distance between consecutive profiles was 100 µm. The algorithm included conversion of the proprietary Keyence 3D image depth representation and storing the converted data as tab-delimited files. These were later analysed using the open-source software tool Gwyddion (gwyddion.net). The 3D surface map processing included the removal of horizontal scars, elimination of abnormal peaks and outliers, and correction of form errors. The processed image was finally exported as a stereolithography (.stl) file, readable by FEM simulation software. At least four representative 3D surface maps were generated for each machining scenario.

To determine surface roughness parameters, three areas (650 × 650 pixels each) were extracted from each 3D map of surface preparation method variation, and the surface topography was evaluated using standard roughness parameters. *Sa* (arithmetical mean height) and *Sq* (root mean square height), which describe the average vertical deviations of the surface from the mean plane. *Sp* and *Sv* represent the height of the highest peak and the depth of the deepest valley, respectively, while *Sz* denotes the total vertical range (*Sp* + *Sv*). *Ssk* (skewness) characterizes the asymmetry of the height distribution, indicating whether the surface profile is dominated by peaks (*Ssk* > 0) or valleys (*Ssk* < 0). *Sku* (kurtosis) describes the sharpness of the surface profile: higher values (*Sku* > 3) indicate the presence of sharp peaks and deep valleys, whereas lower values (*Sku* < 3) suggest a flatter surface with less pronounced features.

2.3 Bonding and testing

After planing and sanding the wood to its final dimensions, surface scanning was performed, immediately followed by the bonding process using a Langzauner LZT-UK-30-L press. Both scanning and bonding were carried out on climatised lamellae within few hours to minimize any changes in surface properties due to moisture exchange or contamination. Therefore, it is assumed that in this uncontrolled climate period, of the bonding process, no major change of properties occurred. The details of the adhesive and bonding conditions are given in Table 1.

The complete testing and bonding procedure is illustrated in Fig. 2. Glued lamellae were stored in a climate-controlled room at 20 °C and 65% relative humidity for one week. Afterward, the specimens were prepared according to the EN 302-1 standard, ensuring precise attention to groove depth. Fifteen specimens per series were tested, and wood failure percentage was evaluated. Mechanical testing was conducted using a Zwick/Roell Z100 universal testing machine, which additionally measured force and displacement values. All failures occurred within 30 to 90 s intervals.

The shear strength (τ) of single-lap adhesive joint was defined as Eq. (1),

$$\tau = F/bl \tag{1}$$

where F is the measured force, b is the overlap width (~20 mm) and l is the overlap length (~10 mm).

2.4 Finite element modeling

The morphological finite element modelling approach started with the preparation and simplification of the geometry of the scanned *.stl files (3D surface maps), which was done in Rhino v6 (rhino3d.com). To study the mechanical interlocking effect of different surface topographies and roughness, the simplified and filtered meshed surface geometries were transformed to 3D solids and imported as *.stl files in COMSOL Multiphysics 5.5 (comsol.com). The implemented continuum mechanics modeling procedure of the adhesive (interfacial) failure is based on widely known principles for adhesive joints; further details on the implemented procedure can be found in He (2011) and Akhavan-Safar (2022). In this regard, a modified local cohesive zone modelling (CZM) approach for interfacial failure analysis was introduced by using a zero-thickness thin elastic layer between the contact pairs which are comprised of evenly distributed non-linear surface springs defined by a bilinear force-extension function, which implicitly simulated the

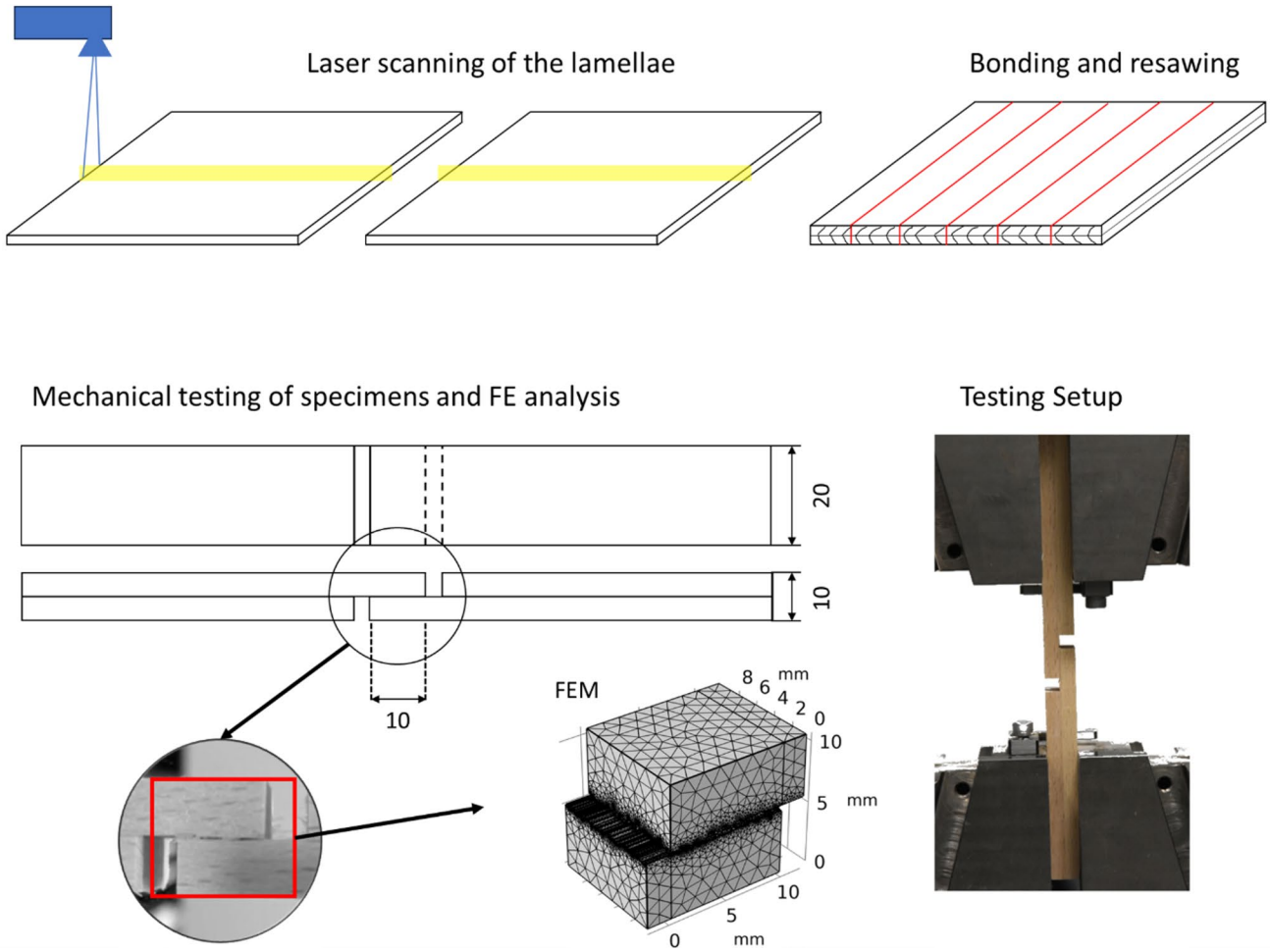

Fig. 2 Process of laser scanning, bonding, subsequent finite element analysis model geometry and mechanical testing of lap joint specimens according to EN 302-1

Table 2 FE models nomenclature with defined surface type, material models and properties used for the analysis

Model Name	Surface Type	Avg. adhesive thickness	№ of elements
FEM I - S1	Ideal smooth surface	0.25 mm	863,109
FEM II - S2	Initial planed surface	0.19 mm	927,669
FEM III - S3	Sanded along grain	0.22 mm	755,409
FEM IV - S4	Sanded across grain	0.24 mm	600,924
Orthotropic elastic material model – beech wood (upper and lower adherend)			
E_L = 13,439, E_R = 1880, E_T = 1031, G_{LR} = 1608, G_{RT} = 460, G_{LT} = 1059 [MPa]			
ν_{LR}=0.073, ν_{RT}=0.360, ν_{LT}=0.043 [−] (Milch et al. 2016)			
Failure index criteria: *Tsai-Wu Orthotropic*			
$\sigma_{L,\,Te}$=114, $\sigma_{R,\,Te}$=8.03, $\sigma_{T,\,Te}$=8.59, $\sigma_{L,\,Co}$=47.5, $\sigma_{R,\,Co}$=9.49, $\sigma_{T,\,Co}$=8.11,			
σ_{LR}=12.6, σ_{RT}=14.2, σ_{LT}=12.6 [MPa] (Milch et al. 2016)			
Isotropic elastic material model – polyurethane adhesive (adhesive layer)			
E_i = 1100 [MPa]			
ν=0.45 [−] (Kläusler et al. 2013)			
Failure index criteria: *Von Mises Isotropic* – $\sigma_{tensile}$ =23.7 [MPa] (Kläusler et al. 2013)			
$\gamma_{f\,yield}$= *1.5 [−]*,$\sigma_{i\,yield}$ =15.9 [MPa], $\sigma_{ij\,yield}$=9.2 [MPa], $\sigma_{y\,Mises}$=27.6 [MPa]			

*E_i is normal elastic modulus, G_{ij} is shear elastic modulus, ν_{ij} is Poisson's ratio, $\sigma_{i,\,Te}$ is yield stress in tension, $\sigma_{i,\,Co}$ is yield stress in compression, σ_{ij} is shear yield stress. Indices i and j characterize anatomical directions L, R, and T (longitudinal, radial, tangential) for the orthotropic material model, and X, Y and Z – directional axes for the isotropic material model, respectively

bilinear traction-separation law (TSL). With this methodology, the adhesive interfacial bond is simulated with nonlinear springs, whereas solid tetrahedral finite elements, with different material models and properties, represent the adherend and adhesive layer, respectively. The model types characteristics and properties considered to define the materials are presented in Table 2, whereas the workflow of the previously described modelling procedure is shown in Fig. 3. The integration of the CZM functions into the FE models using zero-length springs is illustrated in Fig. 4. The figure shows the implementation of the TSL with different constitutive law functions for in-plane tangential shear separation (mode I) and normal or tensile separation (mode II), defined in the local coordinate system. The penalty stiffness (compression), which is not shown due to scale and clarity, was set to 10^5 MPa. The boundary conditions of the models include one end of the lower adherend which is fixed, and the other end of the upper adherend which has an induced prescribed displacement. The FE mesh element type and size used were calibrated for general physics (adaptive function of the software itself) and expected stress concentrations (areas of interest e.g. adhesive and contact points refined to ensure better results), considering time and memory capacity constraints. Finally, to simplify and reduce the number of elements and running time, the models consider the symmetry of the testing procedure by modeling only half of the specimen.

To investigate the influence of varying adherend surface topography on adhesive behaviour, shear strength capacity, and mechanical interlocking, four FE models with different surface topography were developed. Model FEM I – S1 features a completely smooth surface with an adhesive thickness of 0.25 mm, while models FEM II through FEM IV incorporate original (simplified) scanned surfaces with different (planed and sanded) surface preparation methods. The average thickness of the adhesive layer for the scanned surfaces is kept as low as possible ~ 0.2 mm, with regions varying between 0.5 and 0.0 mm, as shown in Fig. 5 for 3D and 2D bondline - thickness profiles and boundaries.

In addition, to mutually compare the global force-displacement behaviour of the tested and modelled specimens, the unmodelled part of the beechwood specimen, between the bonded area and testing device holders - attachment points, was considered to undergo an axial liner deformation, defined as Eq. (2),

$$u_{axial} = F/K_{axial} \tag{2}$$

where F is the obtained loading force and K_{axial} is the axial stiffness of the specimen, calculated by Eq. (3),

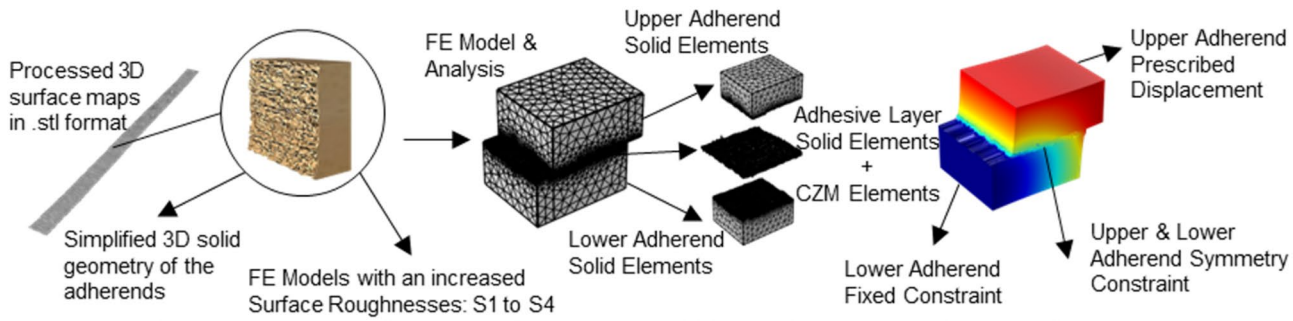

Fig. 3 Morphological FE modeling approach procedure: geometry preparation, model element types and boundary conditions

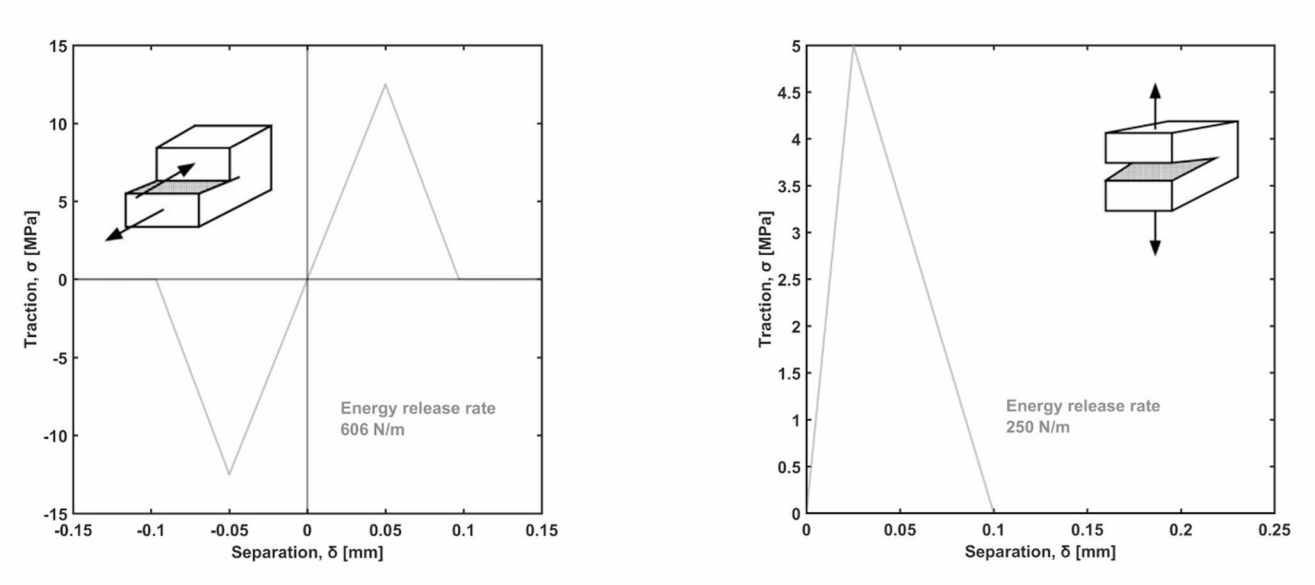

Fig. 4 Adhesive interfacial bond CZM function parameters used for the force per area as a function of extension springs (*left*) Tangential – Shear CZM function (*right*) Normal - Tensile CZM function. Values modified based on the studies by Ammann (2015) and Sebera et al. (2021)

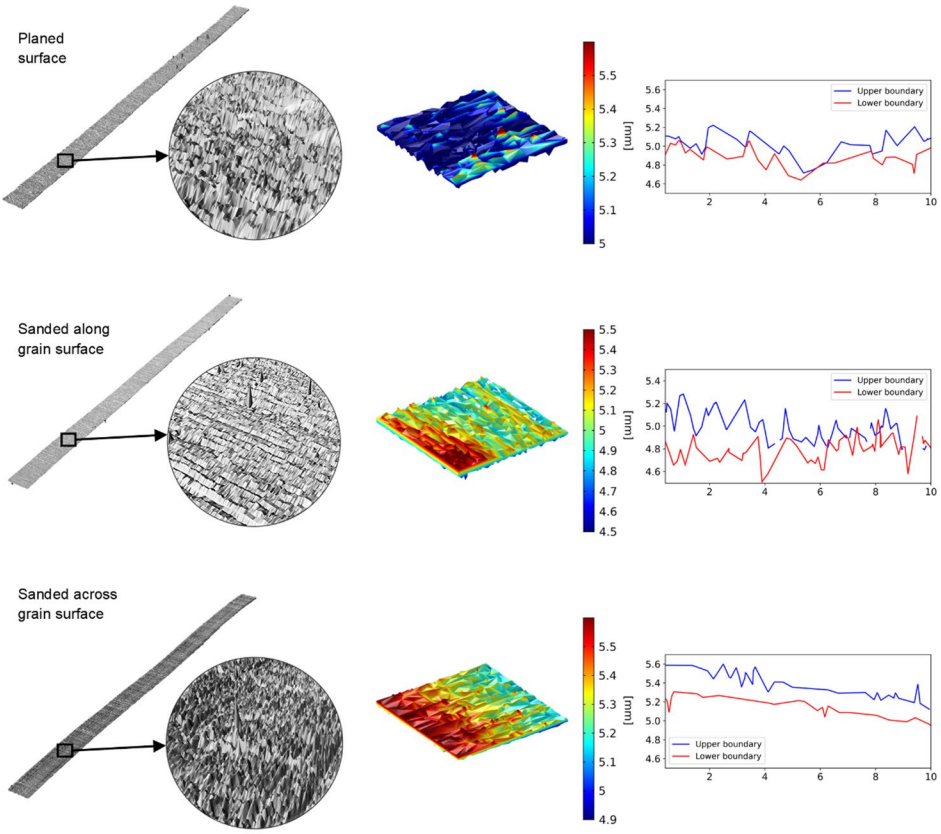

Fig. 5 Implemented treated surfaces – 3D morphology and 2D cross-sectional centre of bondline profiles – adhesive layer thickness of different models (S2 – S4, see Table 2) with surface height represented by colour

$$K_{axial} = E_L A / l_s \quad (3)$$

where E_L is the Elastic beech wood modulus in the longitudinal direction, A is the cross-sectional area (~100 mm^2) and l_s is the unmodelled length of the specimen (~30 mm), whereas a possible out of device holders slip, after the preloading procedure, was considered to be negligible.

3 Results and discussion

The results of the tensile shear strength tests, including wood failure percentage (WFP), and adapted log-normal distribution functions in accordance with the JCSS probabilistic model code resistance models for timber are presented in Fig. 6. Analysis of variance (ANOVA) revealed statistically significant differences among the three tested series ($F = 11.01$, $p < 0.001$). To further analyse the differences, a Tukey post-hoc test was conducted, which showed that the mean values of the planed series and the sanded across grain direction series, as well as the planed series and the sanded along grain direction series, differ significantly. In contrast, the differences between the sanded along grain direction series and the sanded across grain direction series were not statistically significant ($p = 0.2625$). Following, based on average values it can be concluded that sanding of the surface led to an increased shear strength value, although results exhibited a closer spread, which aligns with similar observations made by Bamokina Moanda et al. (2022). Since there was no post-treatment of specimens, shear strengths above 10 MPa were expected. However, shear strength results, particularly for specimens with planed surfaces, are slightly below what is generally reported in the literature. For instance, we achieved shear strength values of approximately 11 MPa for planed surfaces and around 12 MPa to 12.7 MPa for sanded surfaces. Following, these values are somewhat lower compared to those reported by Bamokina Moanda et al. (2022), who found shear strengths around 15 MPa for planed surfaces and around 17 MPa for sanded surfaces. In contrast, Hänsel et al. (2023) reported higher values for planed surfaces, around 16 MPa, but lower values, about 15 MPa, for sanded surfaces. In addition, as mentioned previously, in this context they suggest an upper limit value of roughness, where a positive effect cannot be realized Their study also observed that WFP and tensile shear strength are not correlated, a finding that aligns with our results. In our study, WFP was evaluated for each specimen, with the results reported as mean values: 24% for the planed surface, and 61% and 35% for the sanded surfaces along and across the grain, respectively. Bernaczyk et al. (2023) observed values of 13.5 MPa, and even 14.3 MPa with the inclusion of polyamide fibres. In contrast, Ramachandrareddy et al. (2024) reported values around 11 MPa, closely matching our results for planed surfaces. The density of the wood used in our study (700 ± 20 kg/m³) is comparable to that reported in these studies, suggesting that overall density is not the primary factor behind the observed differences. However, locally denser zones or minor grain and fiber deviations can greatly influence the shear strength of individual specimens. This might partially explain the observed variation within test series, especially for untreated, planed surfaces. Furthermore, the study by Ramachandrareddy et al. (2024) also highlighted that the execution of groove depth significantly influences results, indicating that variations in test procedures, such as specimen rotation or slipping out of holders, can greatly affect tensile shear strength outcomes. Finally, it is important to note that the results discussed here are specific to the use of

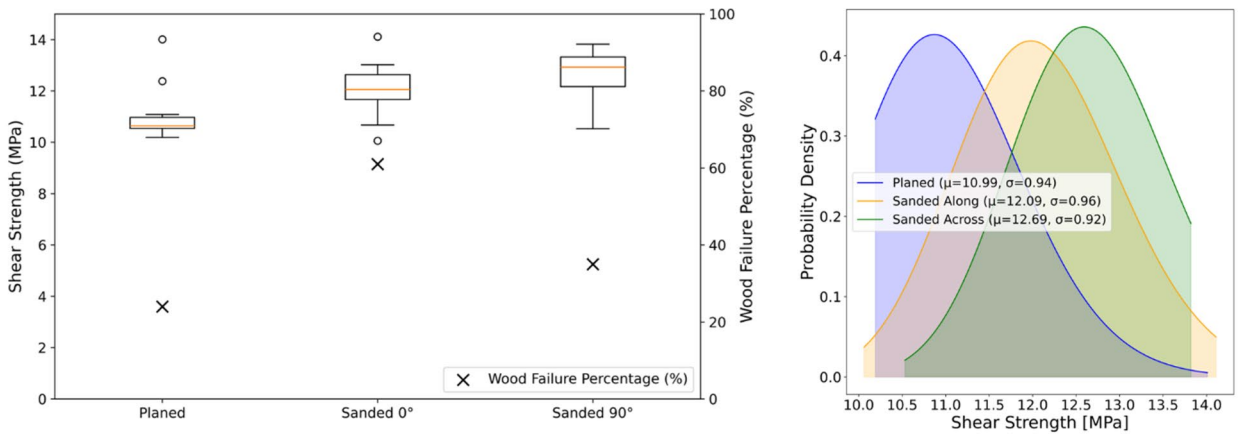

Fig. 6 (*left*) Tensile shear strength test results - white dots outside the box plot represent values that significantly differ from the rest of the data points - outliers. (*right*) Log – normal distribution densities of shear strength test results

Table 3 Surface roughness parameters of all − 54 scanned specimens (Mean – $\mu \pm$ Standard deviation - σ)

Roughness Parameter	Planed surfaces		Sanded 0° surfaces		Sanded 90° surfaces	
-	μ	σ	μ	σ	μ	σ
Sq	19.7	±2.5	31.9	±13.5	27.6	±10.9
Sa	15.5	±2.2	26.5	±12.4	22.9	±9.7
Ssk	-0.1	±0.6	0.1	±0.5	-0.3	±0.3
Sku	0.7	±0.6	1.4	±3.7	0.2	±1.1
Sp	132.3	±68.7	301.2	±126.9	194.8	±106.4
Sv	262.7	±175.6	271.3	±160.6	222.9	±78.3
Sz	395.0	±187.4	572.5	±223.6	417.7	±115.0

*Sq - root mean square height, *Sa* - arithmetical mean height, *Ssk* – skewness, *Sku* – kurtosis, *Sp* - height of the highest peak, *Sv* - depth of the deepest valley and *Sz* - total vertical range

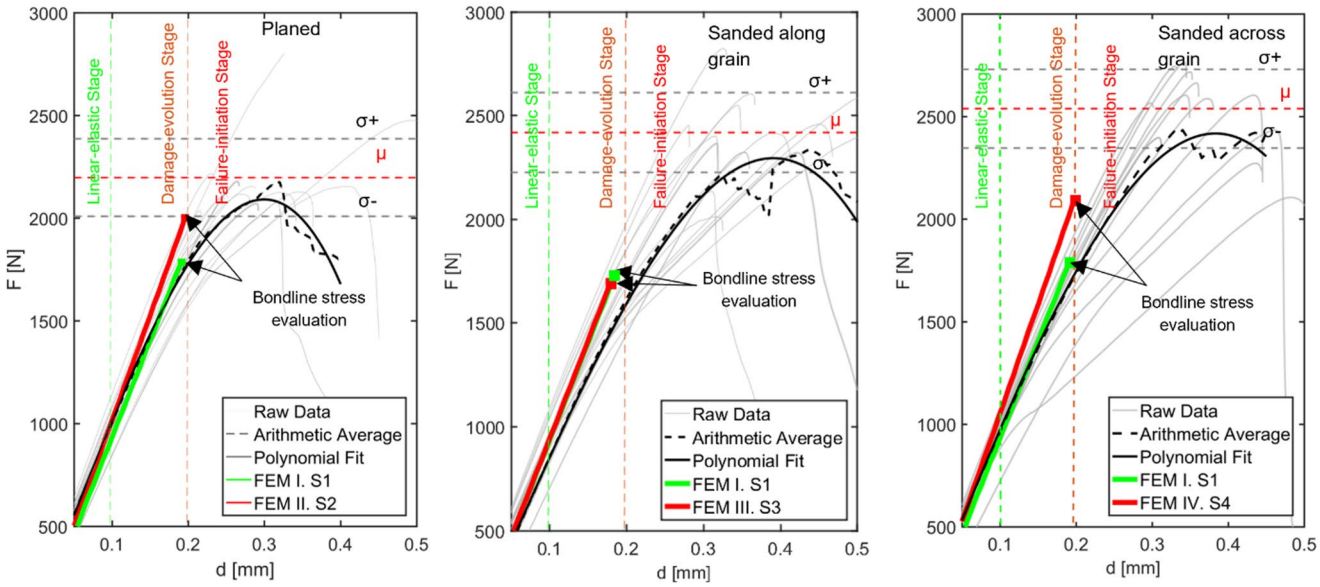

Fig. 7 Experimental and numerical FE model force-displacement curves for the tested planed and sanded specimens

structural PUR adhesive with no pretreatment of the lamellae, such as water spray or primer.

Surface roughness analysis, of all 54 specimens – 18 per surface preparation series, presented in Table 3 shows that planed surfaces had the lowest values of average roughness (*Sa* = 15.5 µm; *Sq* = 19.7 µm), indicating a relatively smooth and homogeneous topography. Sanding notably increased the roughness, especially when performed along the grain (*Sa* = 26.5 µm; *Sq* = 31.9 µm), while sanding across the grain resulted in intermediate values (*Sa* = 22.9 µm; *Sq* = 27.6 µm). Maximum peak height (*Sp*) and total height (*Sz*) followed a similar trend, with the highest values recorded for sanded surfaces. The standard deviation of all roughness parameters was substantially lower for planed surfaces, indicating more uniform texture. Skewness (*Ssk*) values were close to zero for all treatments, suggesting nearly symmetrical height distributions, while kurtosis (*Sku*) values for sanded surfaces—especially parallel to the grain—showed a tendency toward leptokurtic profiles, reflecting sharper peaks and deeper valleys. Finally, while the calculated area roughness parameters cannot be directly compared to the more commonly used 2D roughness profiles and Ra values obtained from stylus-based devices (as used in Hänsel et al. 2023 – P80 grit; Moanda et al. 2022 – P100 grit; Kläusler et al. 2014b – P80 and P120 grit), a clear trend of increased surface roughness resulting from sanding with P120 grit sandpaper can still be observed when compared to the planed surface.

To further investigate the observed trends and understand the underlying behaviour mechanisms, on a global and local level, a numerical model (with varying surfaces), as described in Sect. 2.4 was used. The used models simulate the tensile shear strength and local mechanical interlocking mechanism behaviour of the surfaces with varying roughness. The comparison of experimental and numerical results for the force-displacement curves for different models is shown in Fig. 7. The experimental force-displacement diagrams, show an initial linear behaviour to a certain displacement, where a slight non-linearity occurs. After the slight non-linearity, a second tangent stiffness is reached, with which the force peaks, indicating the maximum

load-bearing capacity of the bonded lap joint. Although, the numerical models reach a comparable initial stiffness (linear-elastic stage) and final load bearing capacity (strength) to the experimental tests, the ultimate displacement is lower, which on the one hand suggests an overestimated second tangent stiffness, related to material nonlinearity and limitations of the model to accurately predict the strength degradation in the failure-initiation stage, and on the other hand fails to incorporate the true linear deformation of the unmodelled part of the wood specimen and possible specimen slip in the mechanical testing device holders. At this point, it is worth mentioning that by modeling only the pure smooth surface, with the described modeling principle, it is likely, that in the case of complete validation with load bearing capacity of experimental results, the true strength parameters of the bilinear constitutive law functions will be overestimated, due to the pure mode I interfacial shear failure and exclusion of the stress concentrations caused by the micro pillars and indentations of the treated surfaces. Therefore, in addition, to the global force-displacement diagrams, a mutual comparison of the local bondline behaviour (cohesive and adhesive forces) of different surface models (S1 – S4) was done with a local stress and strain evaluation at the damage evolution stage.

Observing Fig. 8, it is possible to see the influence of micropillars and indentations – surface topography in general on the local stress distribution in the adhesive layer. Although discreet on global stress distribution, it can be seen that the higher the roughness the higher the local stress concentrations and variations in the adhesive (smooth/treated surface), which results in an increase of initial stiffness. In addition, stress concentrations of single-lap bonded joints, which usually appear at edges, and cause a peeling crack separation of the adhesive from the adherends (pure adhesive failure) (Silva & Ochsner, 2008), because of the weak antistripping force of the adhesive, can be clearly seen in FEM I - S1 (a), where a crack (gap) at the edge later initiates a complete interfacial shear failure of the joint. Contrary, the increase of the adhesive thickness, caused by the indentations in the treated surface (e.g. (b, c)), results in an increase of initial stiffness and bending moment at the edges. With the increase of moment, the joint changes its local stress-state and failure mode to a mixed shear stress and stripping mode where an adhesive failure is followed by a cohesive/material one caused by the stress concentrations, which in turn increases the overall joint capacity. Finally, while adherend stress concentrations are not that pronounced as in the adhesive layer, their presence is also visible.

A more detailed understanding of the influence of surface topography on the internal stress distribution (adhesive and cohesive forces) in the adhesive layer can be obtained by observing Figs. 9 and 10. Meanwhile, a comparison of

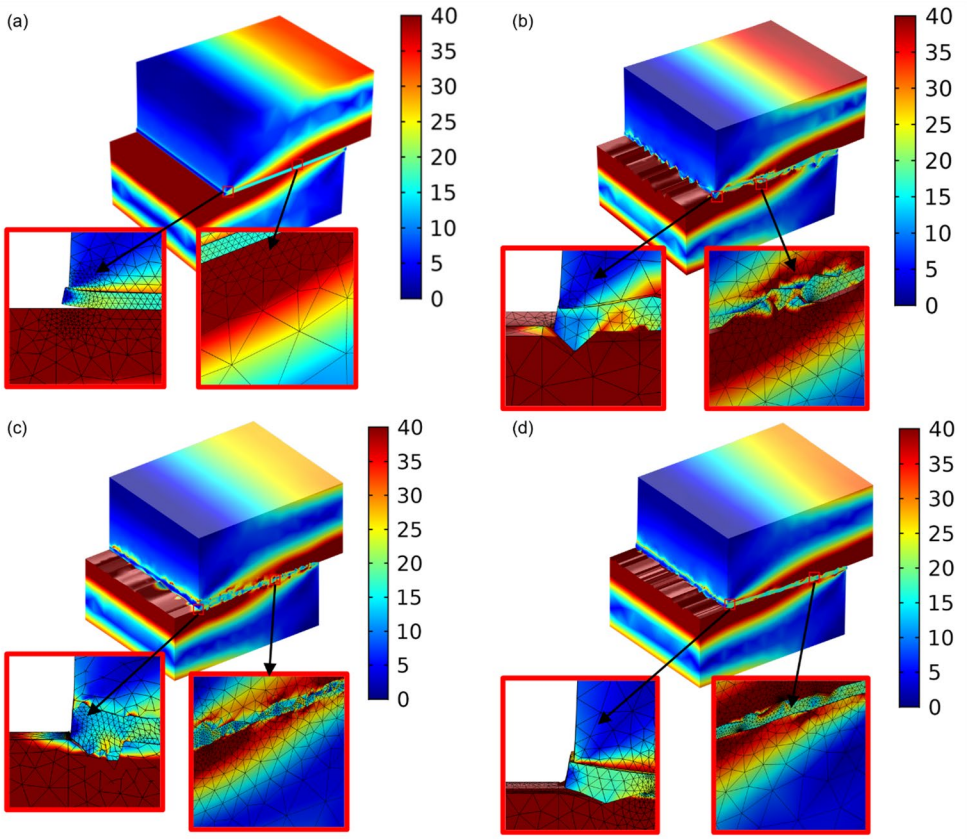

Fig. 8 Global and local (bondline micropillars and indentations) von Mises stress distribution [MPa] for different models at an induced displacement of 0.15 mm (total ~ 0.2 mm) with a deformation scale factor − 2.0: (a) FEM I - S1; (b) FEM II – S2; (c) FEM III – S3 and (d) FEM IV – S4

centre of bondline cohesive shear, normal stress, and strain distribution for different models is shown in Fig. 11. Based on the calculated spatial stress distributions for treated surfaces (S2 – S4) in the adhesive layer, shown in Fig. 9, stress peaks can be clearly distinguished in places with more prominent surface features, however their average centre of bondline von Mises cohesive values tend to be close to each other, in the range of 14.8 to 20.5 MPa. Furthermore, in the case of an ideal smooth surface – S1, stress peaks tend to appear close to bondline edges, whereas in the case of treated surfaces, as expected, their distribution is highly influenced by the surface characteristics. Although, discreet from the point of view of overall global stress distribution, average normal (peel) stresses in the adhesive are slightly reduced for treated surfaces, whereas average shear stresses are slightly higher.

A more prominent effect of surface roughness and its characteristics on stress distribution is noticeable for interfacial adhesive forces, presented in Fig. 10. Nevertheless, despite the distribution change, the absolute stress peaks, for the lower and upper interfacial layer, are again located near bond edges. On this note, by observing the centre of

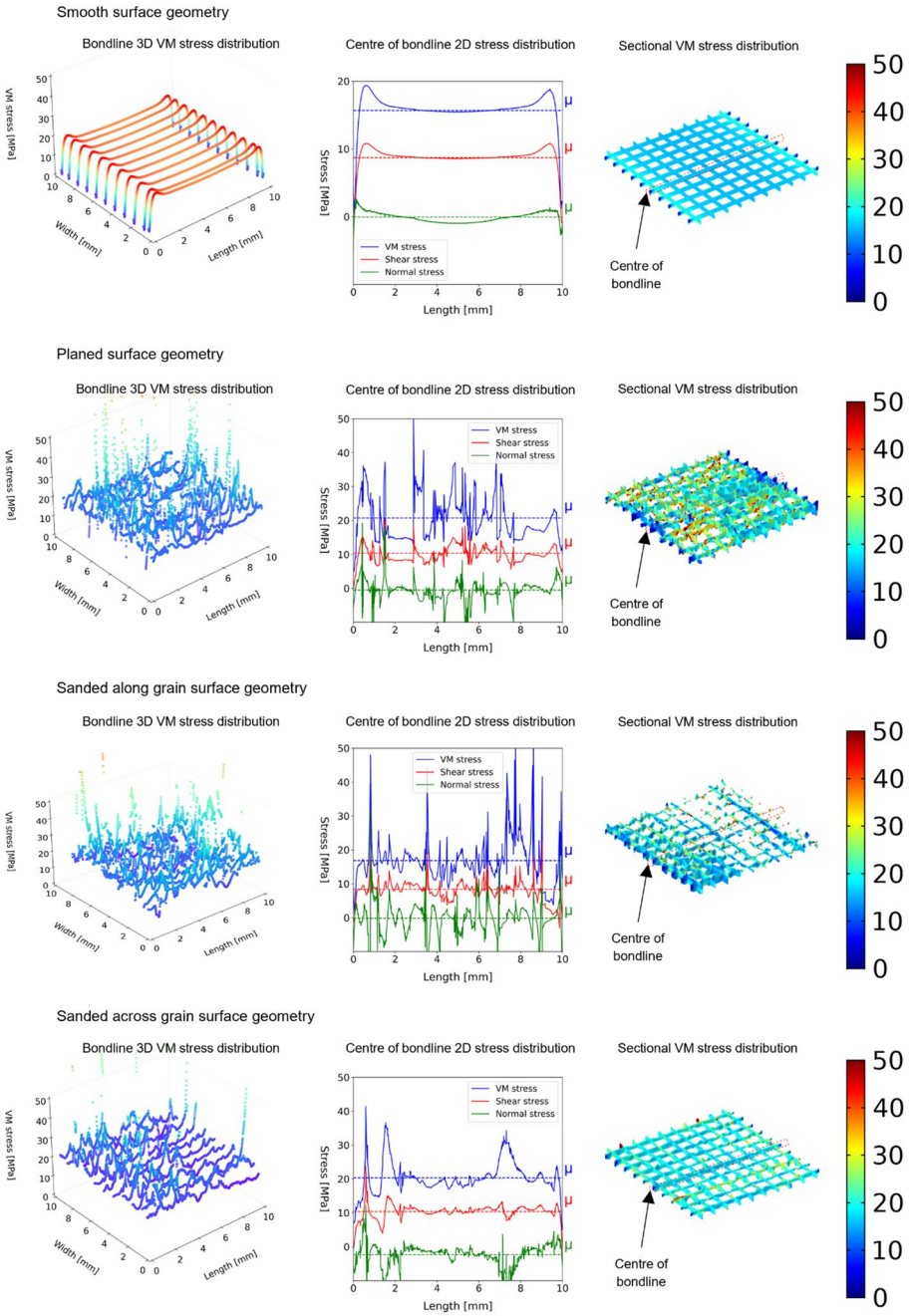

Fig. 9 Adhesive layer stress distributions – cohesive forces of adhesive layer at an induced displacement of 0.15 mm (total ~ 0.2 mm). *VM* – von Mises stress [MPa]

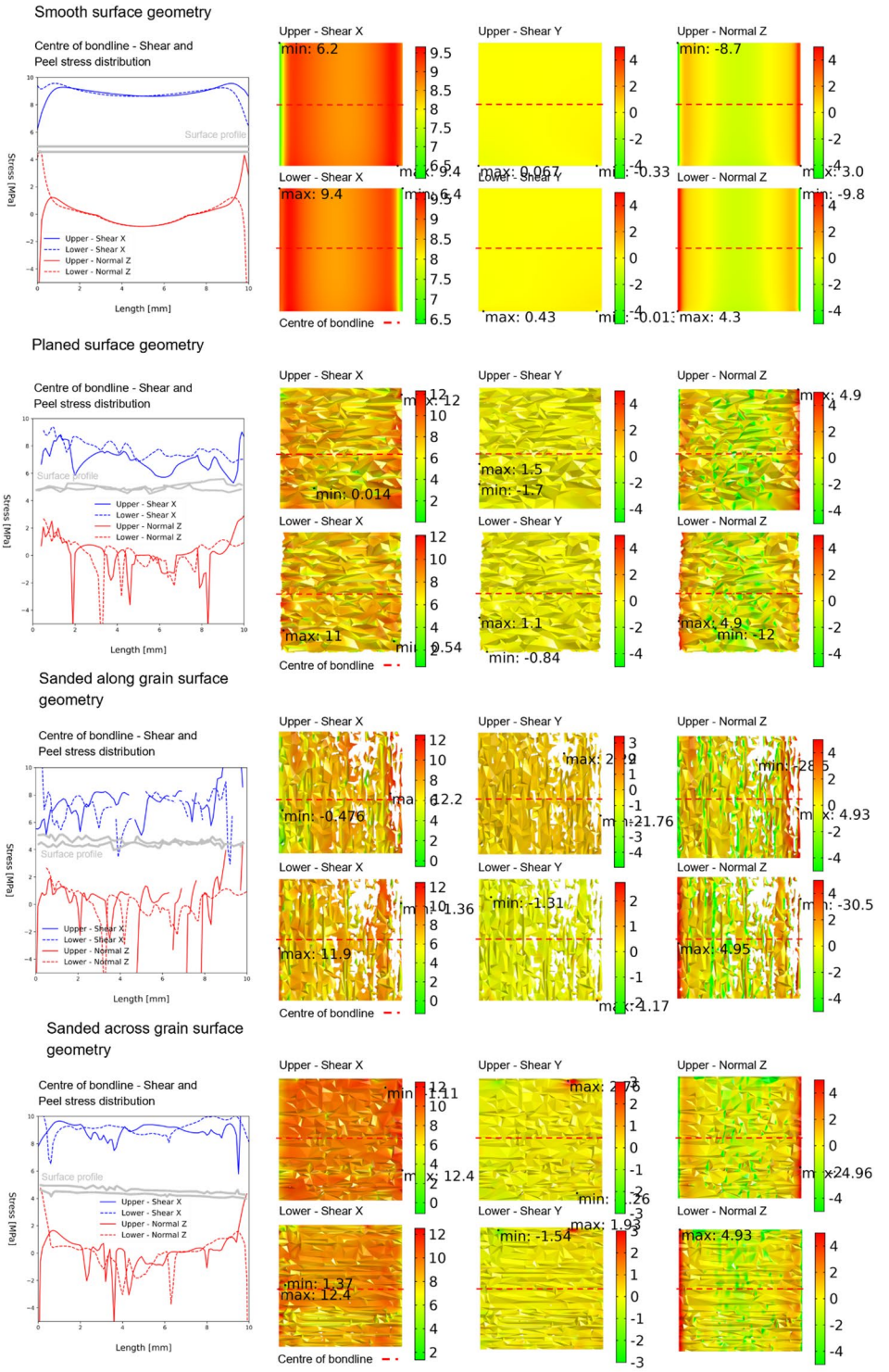

Fig. 10 Upper and lower interface layer adhesive/adherent stress distributions – interfacial adhesive forces per area at an induced displacement of 0.15 mm (total ~ 0.2 mm) in [MPa]

bondline – Shear and Peel (normal) stress distribution plots for the upper and lower adhesive/adherend interface, in combination with the surface profile characteristics (depicted in grey), it can be seen that shear stresses tend to somewhat decrease before micropillars, whereas normal stresses tend to increase. The opposite is true for indentations. At this point, it could be speculated that specimens sanded across grain had an approximately optimal distribution of micropillars and indentations in places of stress peaks in the interface area. Consequently, they had the highest joint strength. In addition, colour map plots show the complete bondline distribution of in-plane tangential shear stresses for the upper

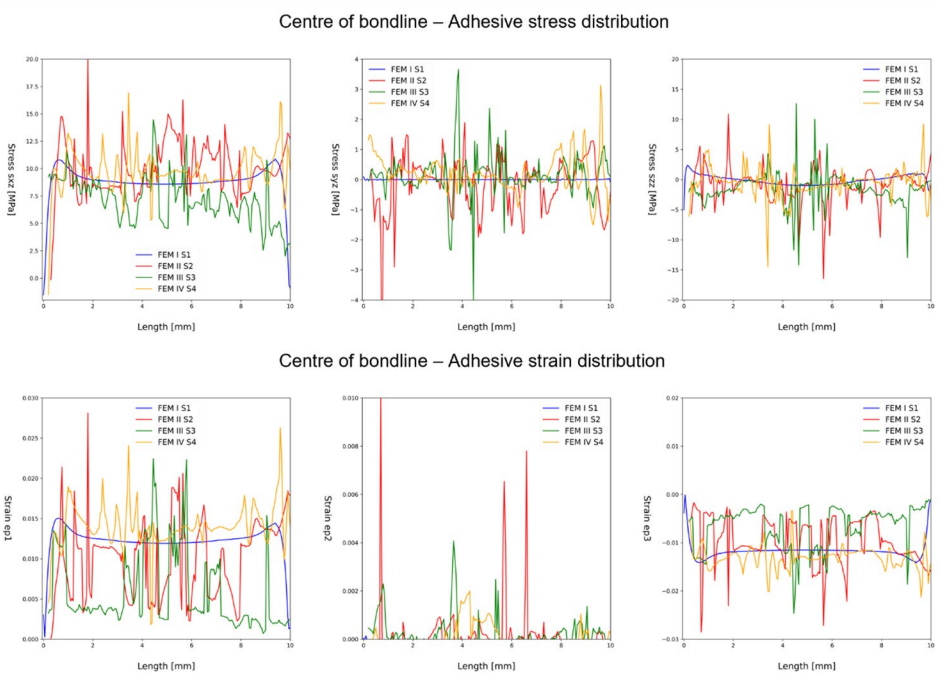

Fig. 11 Comparison of centre of bondline cohesive layer shear and normal stress and strain distribution for different models and surface treatment at an induced displacement of 0.15 mm (total ~ 0.2 mm): *sxz/ep1* – shear along bondline, *syz/ep2* – shear across bondline, *szz/ep3* – normal to bondline

and lower interfacial layer in both X and Y direction, as well as normal or tensile separation stresses in Z direction. Notably, it can be seen that as surface roughness changes from a completely (ideal) smooth surface – S1, in-plane interfacial shear forces in the Y direction start to appear more prominently, however their influence on the global behaviour is limited. Contrary, shear forces in the X direction change their distribution. Finally, treated surfaces normal stresses exhibit higher stress concentrations and a more widespread surface distribution, especially near the central bondline area, when compared to the smooth surface. This, on one hand can be partially attributed to the mechanical interlocking mechanism, especially compressive stresses near micropillars and indentations, where surface characteristics in the central bondline area are more prominent and prone to such an interlocking effect, and on the other hand numerical accuracy caused by difference in stiffness values.

The comparison of cohesive layer stress and strain distribution between different models for centre of bondline, presented in Fig. 11, revealed FEM II – S2 and FEM III – S3 (planed and sanded along grain treatment) as models that exhibit the highest stress and strain variation, indicating significant mechanical interlocking and localised stress concentrations, whereas FEM IV – S4 (sanded across grain treatment) showed moderate variations and high mean values, implying an optimal distribution of stresses throughout the treated surface. Meanwhile, FEM I – S1 (ideal surface) had the most uniform distribution, highlighting the influence of surface roughness on stress and strain distribution and peaks within the adhesive layer. Furthermore, observing the variations and distributions, it can be speculated that, despite the interlocking effect, the presence of certain surface features may prevent a positive overall effect on the joint from being achieved, consequently leading to lower shear strength values, which is in line with the suggested exceedance of the limit value of roughness by Hänsel et al. (2023). In addition, such features may lead to an increase in compressive interlocking stresses in the central bondline area, potentially resulting in a higher percentage of wood failure.

Considering the afore discussion, the results across the four surface models, highlight the difference between varying surface topographies shear and normal stress distribution, and how they impact mechanical behaviour, particularly the shift in stress concentration in the adhesive caused by interlocking. Furthermore, the analysis reveals that stress concentrations and their distribution also increase as surface roughness increases. This is also evident in the adhesive shear stress and normal stress plots, where higher roughness leads to local stress hotspots and shift towards a mixed mode behaviour, caused by crack initiation in the adhesive material. On this note, the models suggest that increased surface roughness enhances mechanical interlocking, while at the same time introducing local failure points for the material – exceeded material strength (cohesive failure pattern). In addition, the failure initiation of the models can be attributed to the topography of the surface, and the adhesive stresses distribution which influences the failure mode to shift more towards a mixed pattern failure. Nevertheless, it is worth mentioning that, on one hand, linear material models may amplify the stress concentration values, whereas on the other hand, achieving numerical

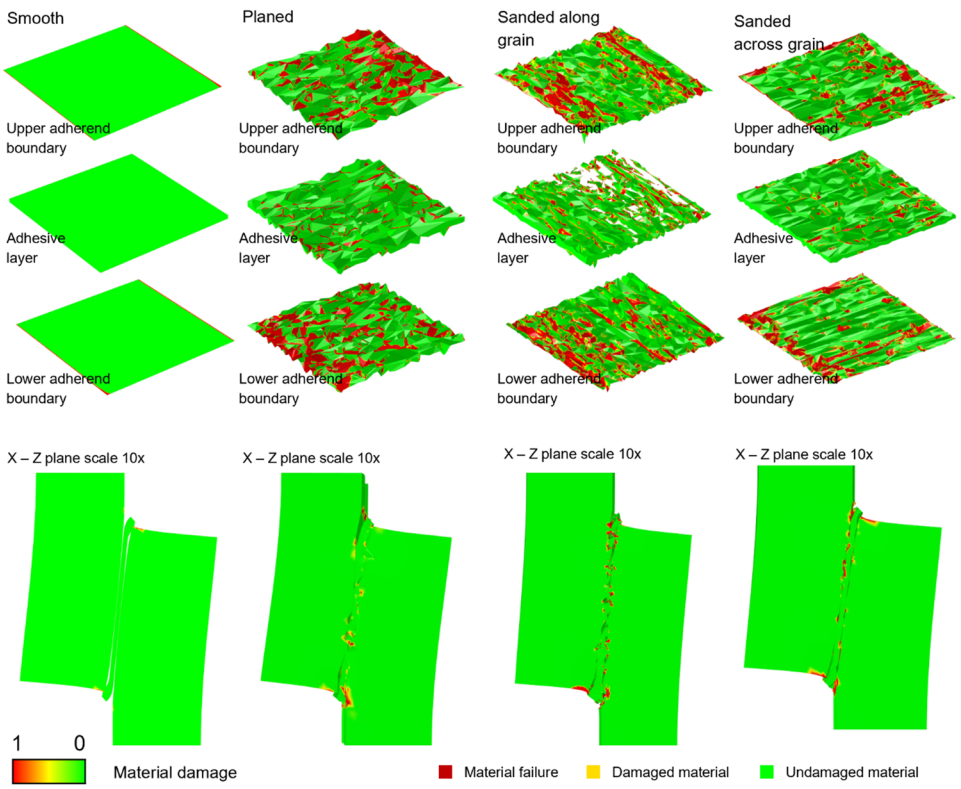

Fig. 12 Damage state of adherend and adhesive for the relevant failure index criteria of the material (see Table 2) at an induced displacement of 0.15 mm (total ~ 0.2 mm): *Undamaged material* – below failure criteria, *Damaged material* – near failure criteria, *Material failure* – above failure criteria or exceeded material strength as per criteria

accuracy in thin regions and complex sharp geometries is proven to be challenging.

The impact of surface topography on the distribution of material damage and degradation within the bonding area, as discussed before, is shown in Fig. 12. Smooth surface exhibits damage localised predominantly at bondline edges, whereas treated surfaces, display a more distributed damage pattern throughout the adhesive and adherend layer. This indicates that optimally treated surfaces increase the energy dissipation of the joint by allowing localised damage of the material, increasing the ultimate displacement, while also altering the failure mechanism, which also aligns with the experimental force-displacement test results. In addition, the failure mode tends to shift towards a more distributed mixed mode failure. This mixed-mode failure is characterized by reduced interfacial shear slip at the bond edge between the adherend and the adhesive, caused by the surface treatment characteristics, somewhat reduced shear stress on one hand, and an increased normal stress on the other. Considering the obtained results, it could be speculated that sanded 90° surfaces promoted an increase in the fragmentation of the adhesive layer during the cohesive part of the mixed failure mode, indicating a modified localised fracture propagation path characterised with an initiation of fracture propagation around the most prominent surface features.

Finally, while surface roughness is often used as a proxy for mechanical interlocking, it represents only a simplified view of a more complex phenomenon. As pointed out by Gardner et al. (2014), mechanical interlocking depends not merely on average roughness values but also on the geometry and distribution of surface features, such as pores, crevices, and micro-indentations, that enable the adhesive to anchor into the adherend. In this study, we acknowledge that statistical profile height alone is insufficient to capture the full extent of adhesive-substrate interactions. Therefore, in addition to roughness quantification and scanning, we employed 3D topographic mapping and morphological FE analysis to study local stress distribution and local failure mechanisms at the bondline. This morphological modeling approach, as discussed, proved to better align with the general mechanical interlocking theory as it accounts for actual surface morphology, including peak shapes and spacing, which could influence adhesive penetration and stress distribution, as well as localisation.

4 Conclusion

Polyurethane adhesive-bonded beech wood single-lap joints tensile shear strength was studied experimentally and numerically using different surface preparation methods. Experimental results showed that sanding across the grain resulted in the highest tensile shear strength with relatively low wood failure percentages. Conversely, the wood failure percentage was highest when sanding along the grain. Planing the surface of the wood yielded the lowest tensile shear strength values, albeit with the least variation in results. 3D scanning of the surface roughness of lamellae prior to bonding successfully detected variations in roughness between different surface preparations and could be linked to higher shear strength as observed in testing. However, it could not be used to accurately predict the mechanical performance and exact influence on the joint in the model. Scanned surface topographies were successfully integrated into the FE analysis program COMSOL Multiphysics, where treated surfaces after the geometry simplification procedure showed higher tensile shear strength and initial stiffness, which was partially attributed to the increased distribution of stress concentrations caused by mechanical interlocking. However, some modelling simplifications and assumptions, in terms of memory capacity and time were necessary, which compromised the accuracy of the model results. In this regard, the biaxial CZM interaction behaviour between the tangential and normal zero-length springs or mixed mode constitutive law and material degradation – nonlinearity, are an additional point which was not addressed in detail, and it could potentially have an influence on the accuracy of the obtained results, especially the second tangent stiffness or near the collapse point of the force-displacement curve. Consequently, primary findings of the implemented finite element morphological method approach are as follows:

(1) The model successfully illustrates the distribution of stresses across the bonding surface area in the initial part of the force-displacement curve (first tangent stiffness and initial adhesive and beech wood damage), where areas of stress concentration and mechanical interlocking can also be observed, which result in an overall increased shear strength capacity and mixed mode behaviour of the joint.
(2) Linear material models cannot accurately capture the damage and strength degradation of beech wood and/or the adhesive material in stress concentration areas, leading to an overestimation of stiffness and stresses values primarily for the second tangent stiffness.
(3) Increased surface roughness may shift the failure mode to a mixed (adhesive-cohesive) failure characterized by a reduced shear slip, which considering the lower stripping strength of the adhesive causes an initiation of a pealing failure at overlap ends. This potentially decreases the overall joint strength once a certain threshold of surface roughness is reached. In addition, it could partially explain why the experimental WFP was not correlated with joint strength or the surface preparation method.
(4) Although, the modeling approach provides insight into the initial stress distribution and global behaviour, it has limitations that must be addressed in future research through further numerical studies and analysis with improved TSL shape for interfacial failure (e.g. trapezoidal or polynomial) and their parameters validation. In addition, it should include a more detailed, in-depth model, which will include penetration of the adhesive bond line, analysed by an optical microscope, and an additional pure cohesive failure or fracture model implemented with simplified CZM or damage elements within the adhesive layer. Finally, to ensure comprehensive and improved validation of results, experimental tests should be conducted with DIC measurements.

Acknowledgements The authors gratefully acknowledge the Slovenian research programs P2-0273 and P4-0430 and research project grants N2-0280, I0-0032 and J4-4546 funded by ARIS – Slovenian Research and Innovation Agency. The financial support by the National Science Centre, Poland under the OPUS call in the Weave programme, No. 2021/43/I/ST8/00554 is also gratefully acknowledged.

Author contributions Material preparation and experimental testing were performed by M.C. and J.S., data analysis by M.C. and L.N., numerical modeling by L.N. The first draft of the manuscript was written by L.N and all authors commented on previous versions of the manuscript. All authors read and approved the final manuscript.

Data availability The data that support the findings of this study are available from the corresponding authors upon reasonable request.

Declarations

Conflict of interest The authors declare no conflict of interests.

References

Akhavan-Safar A, Marques EA, Carbas RJ, da Silva LF (2022) Cohesive zone modelling for fatigue life analysis of adhesive joints. Springer, Gewerbestrasse, Cham, Switzerland, pp 19–42

Ammann SD (2015) Mechanical performance of glue joints in structural hardwood elements (p. 1 Band) [ETH Zurich; Application/pdf]. https://doi.org/10.3929/ETHZ-A-010575524

Ammann S, Schlegel S, Beyer M, Aehlig K, Lehmann M, Jung H, Niemz P (2016) Quality assessment of glued Ash wood for construction engineering. Eur J Wood Wood Product 74(1):67–74. https://doi.org/10.1007/s00107-015-0981-2

Bamokina Moanda D, Lehmann M, Niemz P (2022) Investigation of the impact of Micro-Structuring on the bonding performance of Beechwood (*Fagus sylvatica* L). Forests 13(1):113. https://doi.org/10.3390/f13010113

Bernaczyk A, Wagenführ A, Terfloth C, Lincke J, Krystofiak T, Niemz P (2023) Investigations into the influence of temperature on the tensile shear strength of various adhesives. Materials 16(18):6173. https://doi.org/10.3390/ma16186173

Budhe S, Ghumatkar A, Birajdar N, Banea MD (2015) Effect of surface roughness using different adherend materials on the adhesive bond strength. Appl Adhes Sci 3:1–10

Clerc G, Brunner AJ, Josset S, Niemz P, Pichelin F, Van De Kuilen JWG (2019) Adhesive wood joints under quasi-static and Cyclic fatigue fracture mode II loads. Int J Fatigue 123:40–52. https://doi.org/10.1016/j.ijfatigue.2019.02.008

Da Silva LFM, Öchsner A (eds) (2008) Modeling of adhesively bonded joints. Springer, Berlin, pp 3–22

De Moura MFSF, Oliveira JMQ, Morais JJL, Dourado N (2011) Mixed-mode (I+II) fracture characterization of wood bonded joints. Constr Build Mater 25(4):1956–1962. https://doi.org/10.1016/j.conbuildmat.2010.11.060

EN 302-1:2013-06 (2013) Adhesives for load-bearing timber structures—Test methods—Part 1: determination of longitudinal tensile shear strength. Beuth., Berlin, Germany

Fernandes RMRP, Chousal JAG, De Moura MFSF, Xavier J (2013) Determination of cohesive laws of composite bonded joints under mode II loading. Compos Part B: Eng 52:269–274. https://doi.org/10.1016/j.compositesb.2013.04.007

Gardner DJ, Blumentritt M, Wang L, Yildirim N (2014) Adhesion theories in wood adhesive bonding: A critical review. Reviews Adhes Adhes 2(2):127–156. https://doi.org/10.7569/RAA.2014.097304

Gliszczynski A (2021) Experimental and numerical benchmark study of mode II interlaminar fracture toughness of unidirectional GFRP laminates under shear loading using the end-notched flexure (ENF) test. Composite Structures

Gómez-Royuela JL, Majano-Majano A, Lara-Bocanegra AJ, Xavier J, De Moura MFSF (2022) Evaluation of R -curves and cohesive law in mode I of European Beech. Theoret Appl Fract Mech 118:103220. https://doi.org/10.1016/j.tafmec.2021.103220

Government of the Republic of Slovenia (2023) Regulation on green public procurement (unofficial consolidated text no. 3). Official Gazette of the Republic of Slovenia

Hammerquist CC, Nairn JA (2018) Numerical simulation of pressure-driven adhesive penetration into realistic wood structures. Wood Sci Technol 52(5):1271–1288. https://doi.org/10.1007/s00226-018-1032-z

Hänsel A, Sandak J, Sandak A, Mai J, Niemz P (2022) Selected previous findings on the factors influencing the gluing quality of solid wood products in timber construction and possible developments: A review. Wood Mater Sci Eng 17(3):230–241. https://doi.org/10.1080/17480272.2021.1925963

Hänsel A, Tröger J, Rößler M, Brachhold N, Niemz P (2023) Influence of surface treatment on the bonding quality of wood for load-bearing purposes. Wood Mater Sci Eng 18(6):2128–2139. https://doi.org/10.1080/17480272.2023.2269138

He X (2011) A review of finite element analysis of adhesively bonded joints. Int J Adhes Adhes 31(4):248–264. https://doi.org/10.1016/j.ijadhadh.2011.01.006

Kläusler O, Clauß S, Lübke L, Trachsel J, Niemz P (2013) Influence of moisture on stress–strain behaviour of adhesives used for structural bonding of wood. Int J Adhes Adhes 44:57–65

Kläusler O, Hass P, Amen C, Schlegel S, Niemz P (2014a) Improvement of tensile shear strength and wood failure percentage of 1 C PUR bonded wooden joints at wet stage by means of DMF priming. Eur J Wood Wood Product 72(3):343–354. https://doi.org/10.1007/s00107-014-0786-8

Kläusler O, Rehm K, Elstermann F, Niemz P (2014b) Influence of wood machining on tensile shear strength and wood failure percentage of one-component polyurethane bonded wooden joints after wetting. Int Wood Prod J 5(1):18–26. https://doi.org/10.1179/2042645313Y.0000000039

Konnerth J, Kluge M, Schweizer G, Miljković M, Gindl-Altmutter W (2016) Survey of selected adhesive bonding properties of nine European softwood and hardwood species. Eur J Wood Wood Product 74(6):809–819. https://doi.org/10.1007/s00107-016-1087-1

Luedtke J, Amen C, Van Ofen A, Lehringer C (2015) 1 C-PUR-bonded hardwoods for engineered wood products: influence of selected processing parameters. Eur J Wood Wood Product 73(2):167–178. https://doi.org/10.1007/s00107-014-0875-8

McBain JW, Hopkins DJ (1925) On adhesives and adhesive action. J Phys Chem 29:188–204

Milch J, Tippner J, Sebera V, Brabec M (2016) Determination of the elasto-plastic material characteristics of Norway Spruce and European Beech wood by experimental and numerical analyses. Holzforschung 70:1081–1092

Naat N, Boutar Y, Naïmi S, Mezlini S, Da Silva LFM (2023) Effect of surface texture on the mechanical performance of bonded joints: a review. J Adhes 99(2):166–258

Niemz P, Teischinger A, Sandberg D (eds) (2023) Springer Handbook of Wood Science and Technology. Springer International Publishing. https://doi.org/10.1007/978-3-030-81315-4

Öchsner A (ed) (2008) Modeling of adhesively bonded joints. Springer, Berlin, pp 3–22

Plos M, Fortuna B, Šuligoj T, Turk G (2022) From visual grading and dynamic Modulus of European Beech (*Fagus sylvatica*) logs to tensile strength of boards. Forests 13(1):77. https://doi.org/10.3390/f13010077

Pramreiter M, Grabner M (2023) The utilization of European Beech wood (*Fagus sylvatica* L.) in Europe. Forests 14(7):1419. https://doi.org/10.3390/f14071419

Ramachandrareddy B, Solt-Rindler P, Van Herwijnen H, Wg., Pramreiter M, Konnerth J (2024) Sensitivity of lap-shear test to errors in groove cutting and influence of wood type/treatment. Int J Adhes Adhes 130:103605. https://doi.org/10.1016/j.ijadhadh.2023.103605

Sebera V, Pečnik JG, Azinović B, Milch J, Huč S (2021) Wood-adhesive bond loaded in mode II: experimental and numerical analysis using elasto-plastic and fracture mechanics models. Holzforschung 75(7):655–667. https://doi.org/10.1515/hf-2020-0141

Z-9.1-679 (2018) Glued laminated timber made from Beech wood or Beech hybrid beams for use in structural applications. General building approval